

DoubleDiffusion: Combining Heat Diffusion with Denoising Diffusion for Generative Learning on 3D Meshes

Xuyang Wang¹ Ziang Cheng² Zhenyu Li³ Jiayu Yang² Haorui Ji¹
Pan Ji² Mehrtash Harandi⁴ Richard Hartley¹ Hongdong Li¹

¹ The Australian National University

² Tencent XR Vision Labs

³ King Abdullah University of Science and Technology

⁴ Monash University

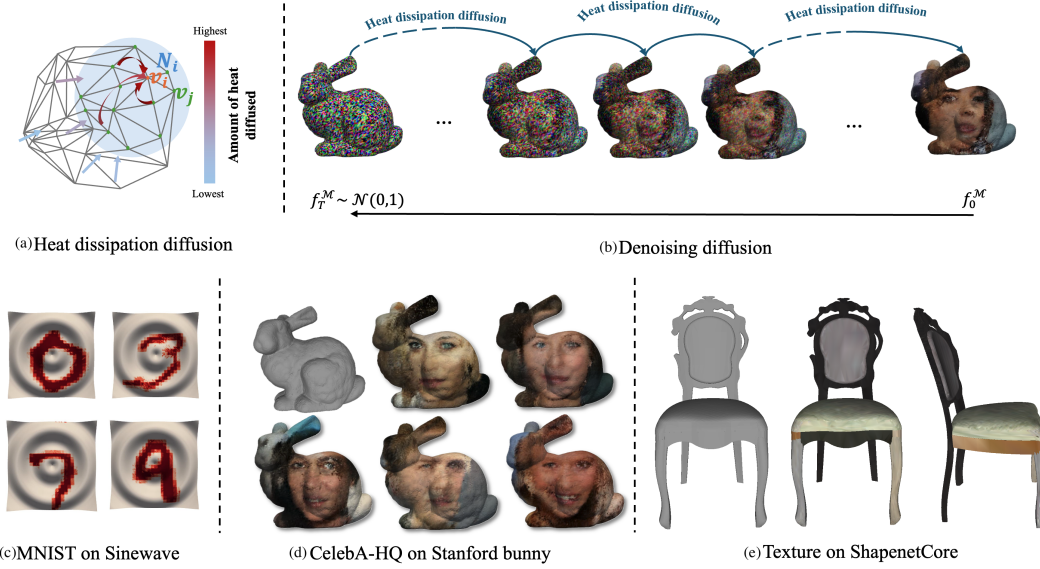


Figure 1. **We present DoubleDiffusion, a framework for generative learning on 3D manifold mesh.** We use (a) the heat dissipation diffusion as the geometric feature extractor to efficiently aggregate vertex features over the spatial domain on mesh surfaces. We employ a (b) temporal denoising diffusion process to capture the distribution of the signal on mesh surfaces. Our model can effectively learn the RGB signal distribution defined on a specific manifold (e.g., (c) sinewave and (d) bunny), to generate different (c) handwritten digits [11] or (d) face looks [18]. Moreover, Our model can generate the texture on different manifold shape given different manifold surfaces from the (e) ShapeNetCore [7].

Abstract

This paper proposes DoubleDiffusion, a novel framework that combines heat dissipation diffusion and denoising diffusion for direct generative learning on 3D mesh surfaces. Our approach addresses the challenges of generating continuous signal distributions residing on a curve manifold surface. Unlike previous methods that rely on unrolling 3D meshes into 2D or adopting field representations, DoubleDiffusion leverages the Laplacian-Beltrami operator to process features respecting the mesh structure. This combination enables effective geometry-aware signal diffusion

across the underlying geometry. As shown in Fig. 1, we demonstrate that DoubleDiffusion has the ability to generate RGB signal distributions on complex 3D mesh surfaces and achieves per-category shape-conditioned texture generation across different shape geometry. Our work contributes a new direction in diffusion-based generative modeling on 3D surfaces, with potential applications in the field of 3D asset generation.

https://github.com/Wxyxixixi/DoubleDiffusion_3D_Mesh

1. Introduction

Significant advancements have been made recently in generative learning using the diffusion probabilistic models [14, 33], particularly in domains involving images [26, 29], videos [6, 15], and 3D such as points clouds [23], tri-planes [32], Nerf [21], mesh texture generation based on grid [22], *etc.* However, the extension of generative learning to 3D object surfaces, typically represented as curved surfaces or manifolds, remains under-explored due to the lack of effective learning strategies on these warped manifold surfaces. Several existing methods [8, 42] attempt to learn the texture distribution on 3D object manifold surfaces through unwrapped 2D texture maps. While these approaches enable surface representation learning in 2D format and can leverage 2D image models to infer texture samples, they often suffer from the inconsistency along edges and fail to fully capture the intricate geometry of the 3D surface. Additionally, unwrapping a 3D surface onto a 2D texture map is ill-posed without a certain solution, thus different unwrapping techniques can significantly impact the final generative results.

While some methods used the point cloud as the manifold surface representation, the neighborhood relationship and the distance are computed through K-nearest neighbors (KNN), the distance are not ideally calculated along the manifold surface [27, 28]. Meanwhile, this approach lacks the precision needed for mesh-based structures, where each point’s neighboring relationships are defined by the mesh’s inherent geometry. Since the mesh is naturally a structured manifold, with the geodesic distance represented via the vertices connectivity, mesh present an ideal medium for diffusion-based generation directly on the surface.

In this work, we present a probabilistic diffusion framework on manifold, addressing the challenge of generative learning directly on the mesh surfaces. Our method captures the local geometric characteristics of 3D shapes without needing to flatten the surface to a 2D medium, ensuring consistency of the content generation across the manifold. Bronstein [5] points out that, Laplacian Beltrami (LB) operator can capture the differential geometric property on the manifold defining neighboring and distance relationship when the information interchanging among the points. To model the diffusion on the manifold mesh surface, we adapt from the mesh processing theory [43] and use the Laplacian Beltrami operator to capture the local geometric of the manifold mesh. Since mesh is a structured manifold, where the geometry of the manifold are explicitly entailed in the mesh topology, the geometric information of the manifold mesh, such as curvatures, geodesic distances of the mesh can be captured and process through the discrete Laplacian-Beltrami Operators [34, 43], opening up a great opportunity to directly learn a scalar distribution defined on the manifold domain.

Specifically, we employ the LB operator as a core feature processing element to approximate heat dissipation diffusion. This diffusion process models the principles of heat transfer on continuous surfaces, where heat spreads over time based on the geometry of the surface, allowing information to propagate across points in a structured manner [9, 13, 31]. On a mesh manifold, the LB operator can approximate this process, effectively simulating heat diffusion and enabling smooth information transfer across vertices. In this paper, we propose to integrate the heat dissipation diffusion with the diffusion probabilistic model [14] as the generative learning framework on the manifold. To our knowledge, we are the first work to combine heat dissipation diffusion with a denoising diffusion probabilistic model (DDPM) for direct learning signal distributions defined on the manifold mesh. We term our framework **DoubleDiffusion**, as it leverages heat dissipation diffusion to capture surface-specific features and employs the diffusion probabilistic framework for generative learning directly on the manifold. In summary, our contributions are:

1. We present DoubleDiffusion, the first framework for denoising diffusion probabilistic model that directly learns and generates signals on the 3D mesh surface, and achieves smoothness and view consistency along the mesh geometry.
2. Our framework achieves a significant 312.82% improvement in coverage compared with the previous SoTA MDF [12]. Meanwhile, it can process large meshes of size *e.g.*, $\sim 100k$ vertices in a single pass, $\sim 20x$ more than MDF. It is also 8.1x faster to generate a sample on the manifold mesh.
3. Experiments on RGB distribution over a single manifold and on per-category shape-conditioned texture generation across multiple shapes demonstrate DoubleDiffusion’s versatility. These results highlight the framework’s capability for geometry-adaptive signal generation on complex 3D surfaces.

2. Related Work

2.1. Differential Geometry and Mesh Processing

In differential geometry, the surface of a 3D mesh is treated as a manifold, making learning over manifolds a longstanding topic of research in mesh processing. Taubin *et al.* [37] proposes using the Laplacian-Beltrami (LB) operator to define differential coordinates on meshes, noting that the integration of these coordinates over a small region approximates the mean curvature at a central point on the manifold. Later, Sörkine *et al.* [34] demonstrates that a mesh’s geometry can be effectively captured using the discrete Laplacian, enabling detailed geometric analysis on non-Euclidean surfaces. [43] indicates that the LB operator offers a robust approach for learning signals over mesh

geometry. Inspired from this, our method follows the geometry processing theory and make use of the mesh Laplacian operators to process the signals over the manifold.

2.2. Diffusion on Manifold

Denoising Diffusion Probabilistic Models (DDPMs) are well-suited for learning on grid-like structured data, where neighborhood relationships are straightforwardly formulated with Euclidean distances. However, limited work has explored DDPMs within the context of manifold geometry. Manifold Diffusion Field (MDF) [12] and Diffusion Probabilistic Field (DPF) [46] address signal generation over the manifold through a field representation with the coordinate-signal pairs. In particular, MDF replaces Cartesian coordinates adopted in DPF with Laplacian eigenvectors to represent manifold geometry, and uses Transformer as the denoising network. Unlike these field-based approaches, our method directly processes signal distributions on manifold, integrating heat dissipation diffusion to capture local geometric dependencies and streamline the generative process.

2.3. Heat Diffusion

The heat equation has been widely applied in message propagation networks, particularly within graph-based deep learning. A closely related work by Xu et al. [41] leverages the heat kernel for semi-supervised learning on graphs, demonstrating that the Laplacian approximation over a heat kernel effectively filters out high-frequency components in node features, thereby enhancing signal smoothness. Similarly, Sharp et al. [31] introduces a heat dissipation diffusion network specifically for mesh structures, providing an ideal tool for our approach. In this work, we integrate the heat diffusion network [31] with a probabilistic diffusion generative model. Here, heat diffusion serves to suppress highly varying components in the noisy feature space, acting as an effective denoiser for the denoising diffusion probabilistic model on meshes.

2.4. Direct 3D Texture Generation

In 3D texture generation, challenges include the limited availability of high-quality 3D datasets and the high computational cost of training general diffusion models on mesh geometries. Some methods attempt to address these issues by projecting multiple views of the 3D object [3, 45] and applying 2D image diffusion models [29, 44] to synthesize signals on the mesh. However, these approaches often result in inconsistency in overlapping regions. Another set of approaches generates content on alternative 3D representations, such as Gaussian Splatting [36], Triplane [39], and Hash-grid [10], with subsequent mesh extraction, which frequently introduces artifacts and reduces quality [10, 36]. Differently, our work addresses these limitations by providing a framework for generating signals directly on 3D

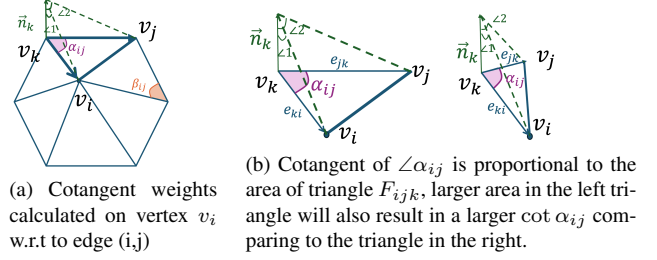


Figure 2. Illustration of the cotangent weighted differential coordinates on the manifold with respect to manifold mesh.

meshes in a way that respects the underlying geometry. This approach enables consistent, geometry-aware generation without the need for view-based projection or post-extraction process, thus preserving mesh integrity and fidelity.

3. Preliminary

3.1. Heat Diffusion

Heat diffusion has long been used in describing how an initial scalar heat distribution \mathbf{h} diffuses or “spread out” over time ‘ s ’. In the differential geometry, it can describe how the signal diffuse over the continuous surfaces. Mathematically, this process is defined as a partial differential equation (PDE):

$$\frac{\partial \mathbf{h}(s)}{\partial s} = \Delta \mathbf{h}(s), \quad (1)$$

where $\mathbf{h}(s)$ represents the feature energy (or heat) over the manifold, s represent the distance of how far the energy is transmitted, and Δ is the Laplacian Beltrami operator characterizes how the temperature at a point diverges from its surrounding region.

3.2. Mesh Laplacian

In the context of 3D mesh, that is, a discrete representation of surface manifolds composed of a finite number of vertices \mathbf{V} and triangular faces $\mathbf{F} \subset \mathbf{V}^3$, we discretize the continuous heat equation to operate on the mesh structure. And we use the cotangent-weighted Mesh Laplacian L^{MC} proposed in [24] as a common practice.

$$\mathbf{L} = \mathbf{M}^{-1} \mathbf{C}. \quad (2)$$

The cotangent weight matrix \mathbf{C} is calculated with respect to the angles adjacent to the shared edges, and the mass matrix is related to the area of the adjacent faces. These reflect the differential relationships and local geometry among vertices, acting similarly to an integration operation over the geodesic neighborhood around each vertex on manifold surfaces [4].

The cotangent weights C are calculated as follows:

$$C_{ij} = \sum_{j \in N(i)} \frac{\cot \alpha_{ij} + \cot \beta_{ji}}{2}, \quad (3)$$

where $C_{ij} \in \mathbb{R}$ represents the cotangent weight along the edge (i, j) , and α_{ij} and β_{ji} are the angles opposite to edge e_{ij} . This formulation considers both edge lengths and adjacent triangle areas (Fig.2), which are loosely related to the Gaussian curvature at the central vertex v_i , as stated in [24].

The cotangent is calculated by:

$$\begin{aligned} \cot \alpha_{ij} &= \frac{\mathbf{e}_{ki} \cdot \mathbf{e}_{jk}}{|\mathbf{n}_k|}, \\ \mathbf{e}_{ki} &= \mathbf{v}_i - \mathbf{v}_k, \mathbf{e}_{jk} = \mathbf{v}_j - \mathbf{v}_k, \mathbf{n}_k = \mathbf{e}_i \times \mathbf{e}_j, \end{aligned} \quad (4)$$

where \mathbf{e}_i and \mathbf{e}_j are the edge vectors.

When angles exceed $\frac{\pi}{2}$, cotangent values become negative. To ensure a positive semi-definite Laplacian matrix, we follow common practice by applying a mass matrix $M \in \mathbb{R}^{n \times n}$, M is a mass matrix given by: $M_{ii} = \frac{1}{3} \sum_{i \in t} \text{Area}(t)$, which assigns one-third of the area of each incident triangle to vertex v_i , thus accounting for the vertex's share of the surrounding area. Having the mass matrix into the cotan-weight Laplacian matrix makes it an FEM Laplacian operator and ensures that its eigenvalue decomposition is robust to mesh parameterization, as discussed in [43].

4. Method

4.1. Overview

Our method begins by computing the cotangent-weighted Laplacian \mathbf{L} from the manifold mesh structure (Sec.3.2), which serves as the foundation for diffusion on the manifold. Using this Laplacian, we perform eigen decomposition on the Laplacian-Beltrami operator, obtaining the smallest k eigenvalues and eigenvectors. These are then used to approximate a heat diffusion kernel $\mathbf{H}(s)$ across the manifold (Sec.4.2).

This heat dissipation diffusion acts as a geometric feature extractor on the manifold, where s in $\mathbf{H}(s)$ represents the distance that a feature diffuses from vertex v_i across the manifold mesh \mathcal{M} . Analogous to a convolutional kernel on an image grid, this heat dissipation diffusion aggregates features on the scalar function \mathbf{f} defined on the vertices of the manifold mesh as $\mathbf{L}\mathbf{f}$. Here, $\mathbf{f} = (\mathbf{f}^{v_0}, \mathbf{f}^{v_1}, \dots, \mathbf{f}^{v_n})$, where \mathbf{f}^{v_i} refers to the scalar vector on vertex v_i , and $\{v_0, v_1, \dots, v_n\} \in \mathcal{M}$.

Our diffusion probabilistic model generates samples by starting with a noise distribution $\mathbf{f}_T^{v_i} \sim \mathcal{N}(0, 1)$, the initial noise is independently sampled at each vertex. The DPM is trained to iteratively predict the reverse transitions $p(\mathbf{f}_T^{v_i} | \mathbf{f}_{T-1}^{v_i})$ progressively denoising through each step.

It's worth noting that, we define two independent parameters: the **heat dissipation diffusion distance** s and the **denoising diffusion time step** t in the DoubleDiffusion framework. The diffusion distance s is a learnable parameter within the heat dissipation network, allowing the model to adaptively capture geometric features on the manifold. In contrast, the denoising diffusion time step t follows a pre-defined schedule, iteratively progressing from T to 0 as part of a recursive Markov chain learning process.

4.2. Laplace Approximation of Heat Diffusion

Solving the heat equation presents an eigenvalue problem, where we can use the mesh Laplacian in Eq. 2 to approximate the heat diffusion. This approach also brings effect to fast compute to the heat diffusion Eq. 1 on large meshes. Meanwhile, Laplacian operators has been recognized as a spectral filter [20, 37]. Choosing the eigenvector of the mesh Laplacian \mathbf{L} with k smallest eigenvalues, Laplacian operator selectively attenuates high-frequency components (sharp changes or noise) while preserving low-frequency components (smooth, global variations). Thus, the Laplacian-approximated heat diffusion functions by dissipating high-frequency variations more quickly than low-frequency components. This behavior effectively smooths the signal, making the heat diffusion process an ideal tool for filtering.

We use the eigen-decomposition of the Laplacian operator in Eq. 2, yielding:

$$\mathbf{L} = \Phi \Lambda \Phi^T, \quad (5)$$

where Φ contains the eigenvectors of \mathbf{L} , and Λ is a diagonal matrix with eigenvalues λ_i . The heat diffusion is then approximated as:

$$\mathbf{H}(s)\mathbf{f} = \Phi e^{-s\Lambda} \Phi^T \mathbf{f} = \sum_{i=1}^k e^{-s\lambda_i} \langle \mathbf{f}, \phi_i \rangle \phi_i. \quad (6)$$

In this spectral representation, the heat diffusion kernel $e^{-s\Lambda}$ has diagonal elements $e^{-s\lambda_i}$ that control the rate of decay for each frequency component.

Furthermore, we followed the method introduce in [31], to apply the heat kernel with respect to the feature channel:

$$\mathbf{H}(s)\mathbf{f} = \Phi \begin{bmatrix} e^{-\lambda_0 s} \\ e^{-\lambda_1 s} \\ \vdots \end{bmatrix} \odot (\Phi^T \mathbf{f}), \quad (7)$$

where the Φ only contains the k smallest eigenvector of the L^{MC} and the eigenvalues are in small to large order $\lambda_0 < \lambda_1 < \dots < \lambda_k$. The symbol \odot represents the element-wise multiplication. In this process, the k -eigenvectors first project the feature signals into the spectral domain, where the high-frequency components are

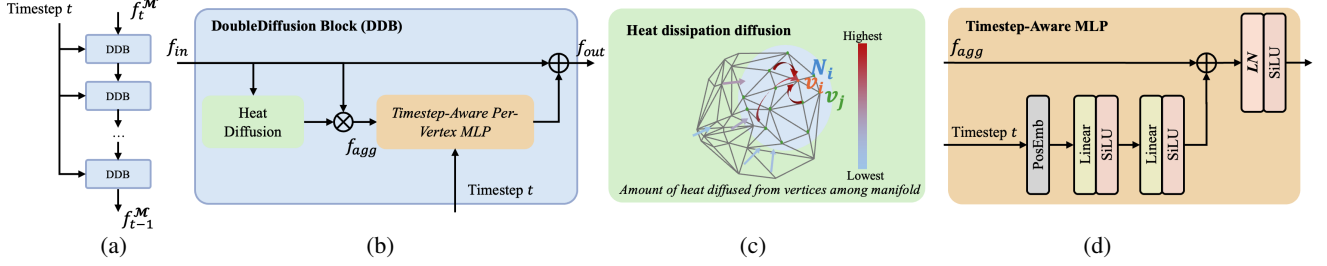


Figure 3. **Framework Overview.** Our (a) DoubleDiffusion Network contains consecutive (b) DoubleDiffusion Blocks (DDB). Each DDB consists of the (c) Heat Diffusion module aggregating vertex features over the spatial domain on mesh surfaces and (d) the Timestep-Aware MLP that injects timestep embedding in a residual manner.

suppressed by the frequency-modulated heat kernel, while low-frequency components are enhanced. This approach achieves channel-wise feature aggregation across vertices in the spectral domain, effectively gathering features within the heat diffusion range defined by the learnable s .

This connection between the heat diffusion equation and low-pass filtering allows us to effectively aggregate features across the manifold while preserving geometric consistency.

Denoising Process with Heat Diffusion. The reverse process $p_\theta(\mathbf{f}_{t-1}|\mathbf{f}_t)$ removes noise iteratively. We parameterize this by predicting the noise $\epsilon_\theta(\mathbf{f}_t, t)$ using the heat diffusion kernel $\mathbf{H}(s)$, where s is the heat diffusion distance:

$$p_\theta(\mathbf{f}_{t-1}|\mathbf{f}_t) = \mathcal{N}(\mathbf{f}_{t-1}; \mu_\theta(\mathbf{f}_t, t), \sigma_t^2 \mathbf{I}), \quad (8)$$

where $\mu_\theta(\mathbf{f}_t, t) = \frac{1}{\sqrt{1-\beta_t}} \left(\mathbf{f}_t - \frac{\beta_t}{\sqrt{1-\alpha_t}} \epsilon_\theta(\mathbf{f}_t, t) \right)$.

Following previous work [30], we incorporate the time step t as a time embedding within each consecutive block using a per-vertex MLP. Given that heat diffusion is conducted on a per-channel basis, employing group normalization [40] directly disrupts the preservation of spatial information, resulting in non-convergence of the model. Consequently, we empirically adopt layer normalization [2] to enhance the training process.

Loss Function. We train by minimizing the MSE loss between the true noise ϵ and predicted noise $\epsilon_\theta(\mathbf{f}_t, t)$:

$$\mathcal{L}_{\text{DDPM}} = \mathbb{E}_{\mathbf{f}_0, \epsilon, t} \left[\left\| \epsilon - \epsilon_\theta(\sqrt{\alpha_t} \mathbf{f}_0 + \sqrt{1-\alpha_t} \epsilon, t) \right\|^2 \right], \quad (9)$$

where $\epsilon \sim \mathcal{N}(0, \mathbf{I})$ and t is sampled from $\{1, \dots, T\}$.

5. Experiments

In this section, we evaluate our proposed framework, **DoubleDiffusion**, for learning signal distributions on 3D mesh manifolds. We conduct three main experiments: (1) learning RGB color distributions on one prescribed manifold Stanford bunny (Sec. 5.1), (2) learning the texture



Figure 4. Qualitative comparison between the (a) MDF (baseline) and (b) DoubleDiffusion (ours) on the Stanford Bunny with $\sim 5k$ number of vertices.

Method	MMD \downarrow	COV \uparrow	#param. \downarrow	t (s) \downarrow
MDF	0.259	7.75	11.4M	1.14
Ours	0.284	32.01	2.4M	0.14

Table 1. Quantity comparison between MDF (baseline) and DoubleDiffusion (ours) with CelebA-HQ on Stanford Bunny (number of vertices $\sim 5k$). With comparable MMD, our method surpasses MDF in terms of COV with a large margin. Meanwhile, our model is 4.7x smaller and 8.1x faster than MDF.

distribution over a set of prescribe manifold and generates diverse textures conditioned on each shape’s geometry (Sec. 5.2). Both tasks are designed to test out the direct generative ability on the manifold as well as the potentials of the proposed method.

5.1. Distribution Generation on Manifold

In this experiment, we evaluate the ability of our framework to learn complex RGB distributions on a 3D curved surfaces. The learning objective is to model the probability distribution $p_\theta(\mathbf{f}_{t-1}^{\mathbf{v}_i}|\mathbf{f}_t^{\mathbf{v}_i})$, where each $\mathbf{v}_i \in \mathcal{M}$, with \mathcal{M} representing the Stanford bunny manifold [38]. Here, $\mathbf{f}_{t-1}^{\mathbf{v}_i}$ is the vertex feature at denoising step $t-1$, with the initial feature $\mathbf{f}_{t=0}^{\mathbf{v}_i}$ being a 3-dimensional RGB value at each vertex acquired from CelebA-HQ human face dataset [18]. This setup allows us to assess the framework’s effectiveness



Figure 5. Our method can efficiently handle the mesh with large number of vertices manifold mesh. Here we show our result with (b) $\sim 25k$ vertices, and (c) $\sim 52k$ vertices (Stanford Bunny), with a qualitative comparison between (a) bunny with $\sim 5k$ vertices. The meshes with higher vertices are watertight remeshing with the off-the-shelf watertight manifold tool ManifoldPlus [16].

in capturing a meaningful distribution over the manifold.

5.1.1. Implementation

Dataset Preparation. As there’s not an available datasets with a large number of texture for one manifold, we follow the baseline method MDF to prepare the manifold value data source from the CelebA-HQ image, as the CelebA-HQ [18] dataset has complex and diverse RGB distributions. Initial RGB values $f_{t=0}^{vi}$ are mapped onto the Stanford bunny manifold using an off-the-shelf texture mapping tool, PyVista [35], which provides a texture coordinate to the Stanford bunny, and we then assigned the per-vertex color values from the image data in CelebA-HQ. Along with the manifold-color pair, we precompute the cotangent-weighted Laplacian matrix for the mesh, along with its eigenvalues and eigenvectors, to facilitate heat diffusion. The CelebA-HQ dataset consists of 30,000 images. We use the official split file with 24,183 images as the training set and 2,824 images as the test set.

Training Details. During training, the network predicts the denoising of RGB values across the manifold. The prediction network utilizes heat diffusion adapted from DiffusionNet [31] as a feature processing mechanism. We employ the EDM [19] framework as the denoising probabilistic model for faster inference with 18 timesteps. All experiments are conducted on 4 NVIDIA A100s, with 96 training epochs, learning rates at $3e-2$, batch size of 8, 128 eigenvector to represent the approximation of the heat dissipation diffusion and 8 DoubleDiffusion blocks. The inference time is evaluated on the NVIDIA A100 GPU.

5.1.2. Evaluation

Baseline and Metrics. Due to the absence of official source code for MDF [12], we meticulously reproduce the baseline MDF method based on the detailed descriptions provided in their paper and its appendix. Specifically, we employed the Transf. Enc-Dec architecture as outlined in the appendix of MDF. We evaluated both MDF and our approach using a manifold-processed and simplified Stanford Bunny model, consisting of approximately 5k vertices [16]. This vertex count is significantly lower than the 50k+ vertices our model is capable of handling. The limitation is due to the computational constraints imposed by MDF’s global attention mechanism, which aggregates features across vertices and escalates computational complexity. For our evaluations, we adopted the metrics proposed by Achlioptas *et al.* [1]: Coverage (COV) and Minimum Matching Distance (MMD). These metrics assess the alignment between the test set and the generated samples, and indicate the accuracy with which the test set is represented within the generated samples, respectively. We followed the implementation from the official code¹ [1] to use the ground-truth and generated samples as reference and sample points, respectively, a practical contrary to that used by MDF. In particular, at equivalent levels of MMD a higher COV is desired [1], and vice-versa. To have a fair comparison, we generate equal number of data samples as the test set to compare the generated distribution with the test distribution.

Comparison. We first present a quantitative comparison in Tab. 1. Although our method posts comparable Minimum Matching Distance (MMD) scores, it achieves a significant 312.82% improvement in Coverage (COV), demonstrating superior alignment between the test-set and generated fields. Additionally, our model is 4.7 times smaller and 8.1 times faster than MDF, highlighting our efficient feature learning that leverages both heat diffusion and denoising diffusion processes. Fig. 4 showcases the qualitative comparison results. Our approach produces textures with enhanced details and more distinct facial features. In contrast, the textures generated by MDF appear excessively smoothed, resulting in a loss of fine details and a uniformly bland, less expressive surface appearance, which we refer to as ‘average faces’. This phenomenon aligns with the quantitative findings, where MDF tends to score better on MMD due to its tendency to predict average-like features thus fails to cover the test-set distribution. This discrepancy can be attributed to MDF’s reliance on Laplacian eigenmaps for spectral positional encodings and its formulation of texture generation as a field. During training, MDF must sample a limited number of points to stay within memory constraints, which may prevent it from fully capturing the un-

¹https://github.com/optas/latent_3d_points/blob/master/notebooks/compute_evaluation_metrics.ipynb



Figure 6. Texture learning across multiple chair shapes in the **ShapeNetCore v2** [7] dataset, with (a) the uncolored chair meshes and, (b) the textured chair meshes sampled from DoubleDiffusion.

derlying geometry. In contrast, our method facilitates local feature aggregation more attuned to the mesh’s shape, resulting in textures that more accurately reflect the surface’s curved structure.

5.1.3. Apply to Larger Meshes

We scaled our experiments to handle larger mesh with 24,992 ($\sim 25k$) and 52,299 ($\sim 52k$) vertices. Fig. 5 demonstrates our method can successfully generate comparatively high-quality textures on these higher-resolution meshes. With the support of more vertices, the generated samples capture better details with less noise. This scalability sheds lights on generative learning over large mesh with complex manifold surfaces, making DoubleDiffusion suitable for applications requiring detailed texture generation over the large number of vertices’ meshes, with a fast speed.

Note that it is *infeasible* for MDF to handle such high-resolution meshes. Facing the limitation of scalability, MDF can be only trained with a maximum of approximately 5,000 vertices on our default GPU. It is due to the adoption of the global attention mechanism to aggregate features at the vertices [25], which has quadratic time and memory complexity. While adopting the advanced framework like PerceiverIO [17] can handle this issue, the performance decreases with the reduce of the number of content points [12, 46]. Moreover, during training, MDF randomly samples points on the mesh surface to facilitate training, which can also hinder the model to learn the underlying complete mesh geometry. In contrast, our method is

specifically designed to learn signal distributions directly on the 3D manifolds by integrating heat dissipation diffusion with a probabilistic model. This combination allows to make a full use of the advantage of heat diffusion to effectively learn on complete mesh shape, and the ability of the denoising diffusion to generate high-quality signals.

5.2. Per-category Texture on ShapeNetCore

In this experiment, we extend DoubleDiffusion to learn over multiple manifold shapes. This setup models the distribution $p_{\theta}(f_{t-1}^{\mathcal{M}_k, v_i} | f_t^{\mathcal{M}_k, v_i})$, where \mathcal{M}_k, v_i denotes vertex v_i on manifold \mathcal{M}_k , with $\mathcal{M}_k \in \{\mathcal{M}_m\}$ representing a set of manifold shapes in the training data. This setup enables DoubleDiffusion to generate textures that are adapted to the structure of each individual mesh in the category, showcasing its capability to handle per-category texture generation across different manifolds.

5.2.1. Dataset and Implementation Details

We use the ShapeNetCore dataset [7] to perform a per-category texture generation. ShapeNetCore is a 3D objects dataset with 55 different categories, such as chairs, caps, cars, etc. Each shape object in the dataset have one corresponding texture. We use the area interpolation to acquire the texture color on the vertices of the shapes, as the texture atlas are defined in per-face manner. As a demonstration, we trained on the “chair” category, which includes 2,412 training samples and 311 test samples. We use the same network setting with the single mesh experiment (Sec. 5.1),

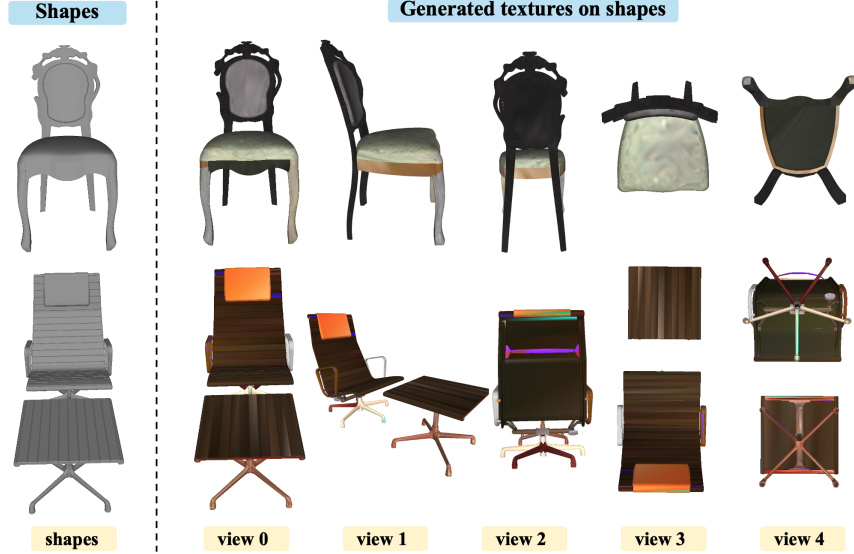


Figure 7. Generative result of the textured chairs from five distinct view points.

only adapt the dataset to handle the batch shape with different number of vertices. To be able to handle shape with large number of vertices, we pad all the shape and related Laplacian matrix to 60,000. During training, we set the batchsize to 4, and train on 4 GPUs for 96 epochs, which is approximately 48 hours.

5.2.2. Qualitative results

Generative qualitative along the geometry. Figure 6 showcases qualitative results from our per-category texture generation experiment on the ShapeNetCore “chair” category. Each column represents a different chair model, where DoubleDiffusion generates textures that adapt to the unique geometric structure of each mesh. The leftmost images in each row show the untextured chair models. Figure 6 demonstrate the qualitative result of texture generation on the different input chairs. The generated color on the mesh are smoothly varying following the chairs geometry, and the generated texture demonstrated a certain level of the understanding to the geometry.

In each example, the generated color on the mesh smoothly varies in alignment with the geometry of the chair, demonstrating the model’s capability to respect and adapt to surface details. Zoomed-in regions highlight the continuity and consistency of the generated textures, especially in curved and intricate parts of the mesh, such as the chair backs, armrests, and legs.

View Consistency. We present the generated results on ShapeNetCore models from five different views in Fig. 7. This multi-view presentation demonstrates DoubleDiffusion’s ability to achieve view consistency in signal generation directly on the mesh, without the need for 2D unrolling

of the mesh. This consistency across views highlights the model’s capacity to respect the underlying mesh structure.

6. Limitation and Future Work

While the multi-view results demonstrate DoubleDiffusion’s strong capability for view-consistent texture generation directly on the mesh, it is also worth noting that our vertex-based approach relies heavily on vertex connectivity and the mesh Laplacian. This reliance can present challenges in accurately capturing color details on large faces, highlighting an area for future refinement in handling textures over varying face sizes on the mesh. Meanwhile, our experiment can only demonstrate the per-category shape conditioned texture generation, lacking the ability to generalize to texture generation on multi-class shapes. The limitation comes from the lack of enough shape-texture data pair, which could potentially be solved by leveraging 2D methods for texture supervision.

7. Conclusion

In this work, we introduced DoubleDiffusion, a novel framework that integrates heat dissipation diffusion with denoising diffusion models to directly generate geometry-respecting signal distributions on 3D meshes. Key contributions include a novel direct learning framework for diffusion on 3D manifold surfaces with the integration of heat dissipation diffusion for effective denoising aligned with mesh structure. We demonstrated that the propose framework performs geometry-adaptive signal generation across multiple complex surfaces.

References

- [1] Panos Achlioptas, Olga Diamanti, Ioannis Mitliagkas, and Leonidas Guibas. Learning representations and generative models for 3d point clouds. In *International conference on machine learning*, pages 40–49. PMLR, 2018. 6
- [2] Jimmy Lei Ba. Layer normalization. *arXiv preprint arXiv:1607.06450*, 2016. 5
- [3] Raphael Bensch, Yanir Kleiman, Idan Azuri, Omri Harosh, Andrea Vedaldi, Natalia Neverova, and Oran Gafni. Meta 3d texturegen: Fast and consistent texture generation for 3d objects. *arXiv preprint arXiv:2407.02430*, 2024. 3
- [4] Alexander M Bronstein, Michael M Bronstein, and Ron Kimmel. *Numerical geometry of non-rigid shapes*. Springer Science & Business Media, 2008. 3
- [5] Michael M Bronstein, Joan Bruna, Yann LeCun, Arthur Szlam, and Pierre Vandergheynst. Geometric deep learning: going beyond euclidean data. *IEEE Signal Processing Magazine*, 34(4):18–42, 2017. 2
- [6] Tim Brooks, Bill Peebles, Connor Holmes, Will DePue, Yufei Guo, Li Jing, David Schnurr, Joe Taylor, Troy Luhman, Eric Luhman, Clarence Ng, Ricky Wang, and Aditya Ramesh. Video generation models as world simulators. 2024. 2
- [7] Angel X Chang, Thomas Funkhouser, Leonidas Guibas, Pat Hanrahan, Qixing Huang, Zimo Li, Silvio Savarese, Manolis Savva, Shuran Song, Hao Su, et al. Shapenet: An information-rich 3d model repository. *arXiv preprint arXiv:1512.03012*, 2015. 1, 7
- [8] Dave Zhenyu Chen, Yawar Siddiqui, Hsin-Ying Lee, Sergey Tulyakov, and Matthias Nießner. Text2tex: Text-driven texture synthesis via diffusion models. *arXiv preprint arXiv:2303.11396*, 2023. 2
- [9] Keenan Crane, Clarisse Weischedel, and Max Wardetzky. Geodesics in heat: A new approach to computing distance based on heat flow. *ACM Transactions on Graphics (TOG)*, 32(5):1–11, 2013. 2
- [10] Kangle Deng, Timothy Omernick, Alexander Weiss, Deva Ramanan, Jun-Yan Zhu, Tinghui Zhou, and Maneesh Agrawala. Flashtex: Fast relightable mesh texturing with lightcontrolnet. *arXiv preprint arXiv:2402.13251*, 2024. 3
- [11] Li Deng. The mnist database of handwritten digit images for machine learning research. *IEEE Signal Processing Magazine*, 29(6):141–142, 2012. 1
- [12] Ahmed A Elhag, Yuyang Wang, Joshua M Susskind, and Miguel Angel Bautista. Manifold diffusion fields. *arXiv preprint arXiv:2305.15586*, 2023. 2, 3, 6, 7, 1
- [13] Alexander Grigoryan. *Heat kernel and analysis on manifolds*. American Mathematical Soc., 2009. 2
- [14] Jonathan Ho, Ajay Jain, and Pieter Abbeel. Denoising diffusion probabilistic models. *Advances in neural information processing systems*, 33:6840–6851, 2020. 2
- [15] Jonathan Ho, William Chan, Chitwan Saharia, Jay Whang, Ruiqi Gao, Alexey Gritsenko, Diederik P Kingma, Ben Poole, Mohammad Norouzi, David J Fleet, et al. Imagen video: High definition video generation with diffusion models. *arXiv preprint arXiv:2210.02303*, 2022. 2
- [16] Jingwei Huang, Yichao Zhou, and Leonidas Guibas. Manifoldplus: A robust and scalable watertight manifold surface generation method for triangle soups. *arXiv preprint arXiv:2005.11621*, 2020. 6
- [17] Andrew Jaegle, Sebastian Borgeaud, Jean-Baptiste Alayrac, Carl Doersch, Catalin Ionescu, David Ding, Skanda Koppula, Daniel Zoran, Andrew Brock, Evan Shelhamer, et al. Perceiver io: A general architecture for structured inputs & outputs. *arXiv preprint arXiv:2107.14795*, 2021. 7
- [18] Tero Karras. Progressive growing of gans for improved quality, stability, and variation. *arXiv preprint arXiv:1710.10196*, 2017. 1, 5, 6
- [19] Tero Karras, Miika Aittala, Timo Aila, and Samuli Laine. Elucidating the design space of diffusion-based generative models. *Advances in neural information processing systems*, 35:26565–26577, 2022. 6
- [20] Bruno Lévy. Laplace-beltrami eigenfunctions towards an algorithm that “understands” geometry. In *IEEE International Conference on Shape Modeling and Applications 2006 (SMI’06)*, pages 13–13. IEEE, 2006. 4
- [21] Chen-Hsuan Lin, Jun Gao, Luming Tang, Towaki Takikawa, Xiaohui Zeng, Xun Huang, Karsten Kreis, Sanja Fidler, Ming-Yu Liu, and Tsung-Yi Lin. Magic3d: High-resolution text-to-3d content creation. In *Proceedings of the IEEE/CVF Conference on Computer Vision and Pattern Recognition*, pages 300–309, 2023. 2
- [22] Zhen Liu, Yao Feng, Michael J Black, Derek Nowrouzezahrai, Liam Paull, and Weiyang Liu. Meshdiffusion: Score-based generative 3d mesh modeling. *arXiv preprint arXiv:2303.08133*, 2023. 2
- [23] Shitong Luo and Wei Hu. Diffusion probabilistic models for 3d point cloud generation. In *Proceedings of the IEEE/CVF conference on computer vision and pattern recognition*, pages 2837–2845, 2021. 2
- [24] Mark Meyer, Mathieu Desbrun, Peter Schröder, and Alan H Barr. Discrete differential-geometry operators for triangulated 2-manifolds. In *Visualization and mathematics III*, pages 35–57. Springer, 2003. 3, 4
- [25] Thomas W Mitchel, Carlos Esteves, and Ameesh Makadia. Single mesh diffusion models with field latents for texture generation. In *Proceedings of the IEEE/CVF Conference on Computer Vision and Pattern Recognition*, pages 7953–7963, 2024. 7
- [26] Dustin Podell, Zion English, Kyle Lacey, Andreas Blattmann, Tim Dockhorn, Jonas Müller, Joe Penna, and Robin Rombach. Sdxl: Improving latent diffusion models for high-resolution image synthesis. *arXiv preprint arXiv:2307.01952*, 2023. 2
- [27] Charles R Qi, Hao Su, Kaichun Mo, and Leonidas J Guibas. Pointnet: Deep learning on point sets for 3d classification and segmentation. In *Proceedings of the IEEE conference on computer vision and pattern recognition*, pages 652–660, 2017. 2
- [28] Charles Ruizhongtai Qi, Li Yi, Hao Su, and Leonidas J Guibas. Pointnet++: Deep hierarchical feature learning on point sets in a metric space. *Advances in neural information processing systems*, 30, 2017. 2

- [29] Robin Rombach, Andreas Blattmann, Dominik Lorenz, Patrick Esser, and Björn Ommer. High-resolution image synthesis with latent diffusion models. In *Proceedings of the IEEE/CVF conference on computer vision and pattern recognition*, pages 10684–10695, 2022. [2](#), [3](#)
- [30] Robin Rombach, Andreas Blattmann, Dominik Lorenz, Patrick Esser, and Björn Ommer. High-resolution image synthesis with latent diffusion models. In *Proceedings of the IEEE/CVF conference on computer vision and pattern recognition*, pages 10684–10695, 2022. [5](#)
- [31] Nicholas Sharp, Souhaib Attaiki, Keenan Crane, and Maks Ovsjanikov. Diffusionnet: Discretization agnostic learning on surfaces. *ACM Transactions on Graphics (TOG)*, 41(3): 1–16, 2022. [2](#), [3](#), [4](#), [6](#), [1](#)
- [32] J Ryan Shue, Eric Ryan Chan, Ryan Po, Zachary Ankner, Jiajun Wu, and Gordon Wetzstein. 3d neural field generation using triplane diffusion. In *Proceedings of the IEEE/CVF Conference on Computer Vision and Pattern Recognition*, pages 20875–20886, 2023. [2](#)
- [33] Yang Song, Jascha Sohl-Dickstein, Diederik P Kingma, Abhishek Kumar, Stefano Ermon, and Ben Poole. Score-based generative modeling through stochastic differential equations. *arXiv preprint arXiv:2011.13456*, 2020. [2](#)
- [34] Olga Sorkine. Laplacian mesh processing. *Eurographics (State of the Art Reports)*, 4(4):1, 2005. [2](#), [3](#)
- [35] Bane Sullivan and Alexander Kaszynski. PyVista: 3D plotting and mesh analysis through a streamlined interface for the Visualization Toolkit (VTK). *Journal of Open Source Software*, 4(37):1450, 2019. [6](#), [1](#)
- [36] Jiaxiang Tang, Zhaoxi Chen, Xiaokang Chen, Tengfei Wang, Gang Zeng, and Ziwei Liu. Lgm: Large multi-view gaussian model for high-resolution 3d content creation. In *European Conference on Computer Vision*, pages 1–18. Springer, 2025. [3](#)
- [37] Gabriel Taubin. A signal processing approach to fair surface design. In *Proceedings of the 22nd annual conference on Computer graphics and interactive techniques*, pages 351–358, 1995. [2](#), [4](#)
- [38] Greg Turk and Marc Levoy. The stanford 3d scanning repository, 1994. [5](#)
- [39] Zhengyi Wang, Yikai Wang, Yifei Chen, Chendong Xiang, Shuo Chen, Dajiang Yu, Chongxuan Li, Hang Su, and Jun Zhu. Crm: Single image to 3d textured mesh with convolutional reconstruction model. *arXiv preprint arXiv:2403.05034*, 2024. [3](#)
- [40] Yuxin Wu and Kaiming He. Group normalization. In *Proceedings of the European conference on computer vision (ECCV)*, pages 3–19, 2018. [5](#)
- [41] Bingbing Xu, Huawei Shen, Qi Cao, Keting Cen, and Xueqi Cheng. Graph convolutional networks using heat kernel for semi-supervised learning. *arXiv preprint arXiv:2007.16002*, 2020. [3](#)
- [42] Xin Yu, Peng Dai, Wenbo Li, Lan Ma, Zhengzhe Liu, and Xiaojuan Qi. Texture generation on 3d meshes with point-uv diffusion. In *Proceedings of the IEEE/CVF International Conference on Computer Vision*, pages 4206–4216, 2023. [2](#)
- [43] Hao Zhang, Oliver Van Kaick, and Ramsay Dyer. Spectral mesh processing. In *Computer graphics forum*, pages 1865–1894. Wiley Online Library, 2010. [2](#), [4](#)
- [44] Lvmin Zhang, Anyi Rao, and Maneesh Agrawala. Adding conditional control to text-to-image diffusion models. In *Proceedings of the IEEE/CVF International Conference on Computer Vision*, pages 3836–3847, 2023. [3](#)
- [45] Longwen Zhang, Ziyu Wang, Qixuan Zhang, Qiwei Qiu, Anqi Pang, Haoran Jiang, Wei Yang, Lan Xu, and Jingyi Yu. Clay: A controllable large-scale generative model for creating high-quality 3d assets. *ACM Transactions on Graphics (TOG)*, 43(4):1–20, 2024. [3](#)
- [46] Peiye Zhuang, Samira Abnar, Jiatao Gu, Alex Schwing, Joshua M Susskind, and Miguel Angel Bautista. Diffusion probabilistic fields. In *The Eleventh International Conference on Learning Representations*, 2023. [3](#), [7](#)

DoubleDiffusion: Combining Heat Diffusion with Denoising Diffusion for Generative Learning on 3D Meshes

Supplementary Material

In this supplementary material, we provide additional implementation details in Appendix A, theoretical analysis in Appendix B and qualitative results in Appendix C.

A. Implementation Details

To give more precise description to the framework in Fig. 3, we have include the diagram to the detail implementation for data preparation in Fig. S1 and heat diffusion block in Fig. S2.

A.1. Input data preparation

To process the mesh structure, we begin by computing the cotangent-weighted Laplacian matrix as discussed in Sec. 4.1. Using eigenvalue decomposition, we then derive its eigenvalues and eigenvectors. Additionally, we compute the mass matrix and the X - and Y -basis vectors for the tangent plane at each vertex. These tangent plane bases can be utilized to scale the heat-diffused features via tangent gradients, following the approach outlined in [31].

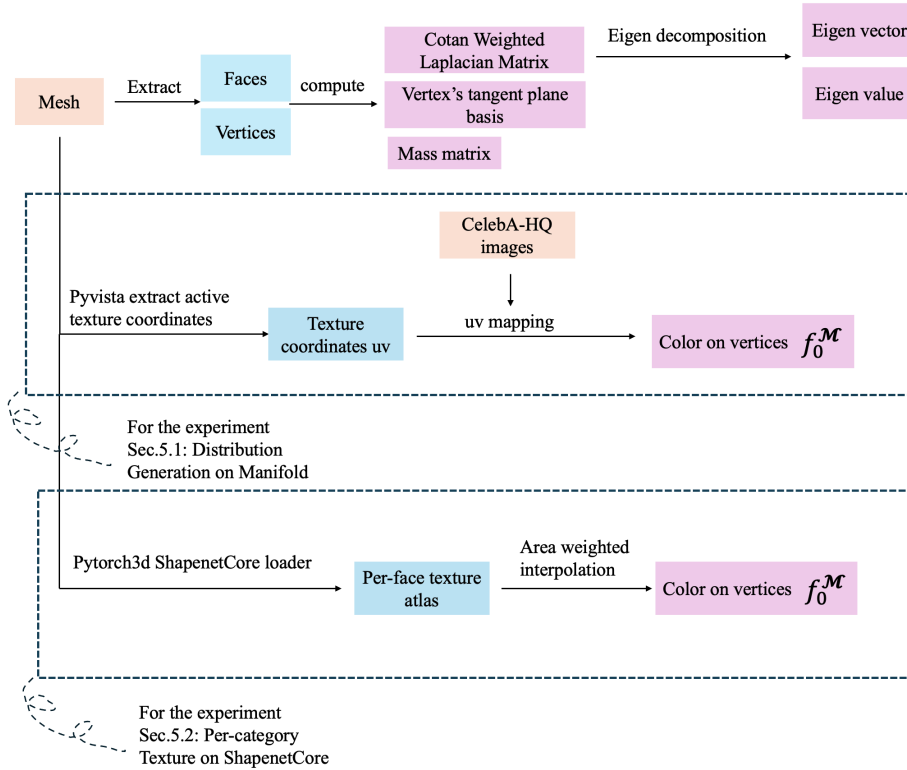


Figure S1. Detail implementation of the input data preparation, for both mesh structure data and the vertex color data.

The extraction of vertex colors is crucial to our experiments, as no existing 3D dataset provides hundreds or thousands of color data points defined on a single mesh structure. Therefore, we follow the baseline experiments [12] to generate the color data distribution using the Stanford Bunny mesh. This process involves employing the off-the-shelf 3D visualization tool PyVista [35] to obtain texture coordinates for the vertices of the Stanford Bunny mesh. With these texture coordinates, we perform UV mapping to transfer image data from the CelebA-HQ dataset, resulting in a mapped color vector assigned to the vertices of the mesh.

For the ShapeNetCore dataset, we utilize PyTorch3D [?] to load the texture atlases corresponding to shapes in the chair category. In PyTorch3D, textures are represented as atlases associated with the mesh faces. To obtain vertex colors from these face-based textures, we perform weighted interpolation. Specifically, for each vertex, we identify all the triangular faces that include it. The area of each triangle is computed, and the texture colors of these triangles are weighted proportionally to their respective areas relative to the total area of all triangles containing the vertex. This ensures accurate color interpolation at the vertex level.

A.2. Implementation of Heat Diffusion Block

The computation of heat-diffused features on the mesh is illustrated in Fig. S2. This process takes place within the heat diffusion block, corresponding to sub-block (c) in Fig. 3. Here, the noised vertex color features are first weighted by the mass matrix to account for the areas of the surrounding faces. The weighted features are then transformed into the spectral domain using the eigenvectors of the mesh structure. In this domain, the features are scaled by heat diffusion coefficients, enabling adaptive learning of geometric features on the mesh.

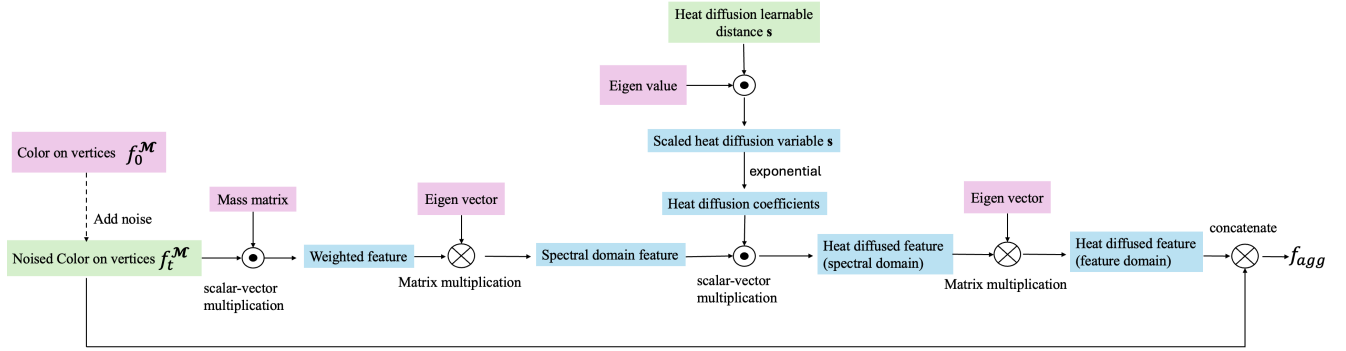


Figure S2. Implementation details of the heat diffusion block

Next, the heat-diffused features are projected back to the original feature domain and concatenated with the noised color features to produce an aggregated feature. This aggregated feature is then passed to the Timestep-Aware Per-Vertex MLP, as depicted in block (d) of Fig. 3, to perform probabilistic denoised diffusion.

B. Theoretical Analysis

In this section, we would like to provide more detail to justify why and how Laplacian Beltrami operator can be used for learning on the manifold surface.

B.1. Integral on the manifold

The intension of using the Laplacian Beltrami operator on the manifold and the mesh is arise from the laplacian's integration formulation on the manifold surface, as advised in the Mesh Laplacian Processing [34].

To analyze and process scalar functions defined on a manifold, the Laplace-Beltrami operator provides a framework for differential and integral operations, analogous to how convolutional kernels operate in the image domain. Since a manifold is locally Euclidean, Sörkine [34] demonstrated that points on the manifold can be represented by differential coordinates δ , which are conceptually similar to Δx in one-dimensional Euclidean space:

$$\begin{aligned}\delta_i &= \mathbf{v}_i - \frac{1}{d_i} \sum_{j \in N(i)} \mathbf{v}_j \\ &= \frac{1}{d_i} \sum_{j \in N(i)} (\mathbf{v}_i - \mathbf{v}_j),\end{aligned}\tag{S1}$$

where d_i is a weighted factor representing the degree of the vertex i , which is the number of connection of vertex i . $N(i)$ represent the neighboring vertex \mathbf{v}_j of the vertex i , it can also be a cotangent weights as a common practice in manifold mesh

processing (Sec 3.2). It's worth noting that, if we take differential coordinates to the continuous form,

$$\lim_{|\gamma| \rightarrow 0} \frac{1}{|\gamma|} \int_{v \in \gamma} (v_i - v) dl(v) = -\text{Curv}(v_i) \mathbf{n}_i. \quad (\text{S2})$$

Eq.(S1) becomes an integration of vertex v_i among the infinite small region within the surface curve γ with perimeter $|\gamma|$, and v are the points that lies in this infinite small closed surface curve. And the $\text{Curv}(v_i)$ in right hand side of Eq.(S2) represent the mean curvature [34] at vertex v_i , and \mathbf{n}_i is the surface normal.

These differential coordinates can be fastly computed through laplacian beltrami operator as it is a discretization version of the integration operator on the manifold, where the differential geometry on the mesh is given by:

$$L = I - D^{-1}A, \quad (\text{S3})$$

where $I \in \mathcal{R}^{n \times n}$ is the identity matrix, $D \in \mathcal{R}^{n \times n}$ is the diagonal matrix with the entries D_{ii} representing the number of the connections of the neighboring vertices (degree). $A \in \mathcal{R}^{n \times n}$ is the adjacency matrix, $A_{ij} = 1$ when the edge exists between vertex i and j .

By incorporating geodesic distance and the area of adjacent triangles, the differential coordinates on the manifold (Eq. S1) with respect to a central vertex can be reformulated using cotangent weights as:

$$\delta_{ij} = \sum_{j \in N(i)} \frac{\cot \alpha_{ij} + \cot \beta_{ji}}{2} (v_i - v_j) \quad (\text{S4})$$

where α_{ij} and β_{ji} are the angles opposite the edge connecting vertices i and j in the triangles adjacent to this edge, these are illustrated in Fig. 2a. Thus, the use of the cotangent weighted Laplacian matrix in Eq. (2) and Eq. (3) upon the manifold surface gives as the geometric properties of the mesh structure.

C. Experiment Results

In this section, we provides additional experiment results for per-category shape conditioned texture generation result on other categories, such as trains Fig. S3, pianos Fig. S4 and faucets Fig. S5.

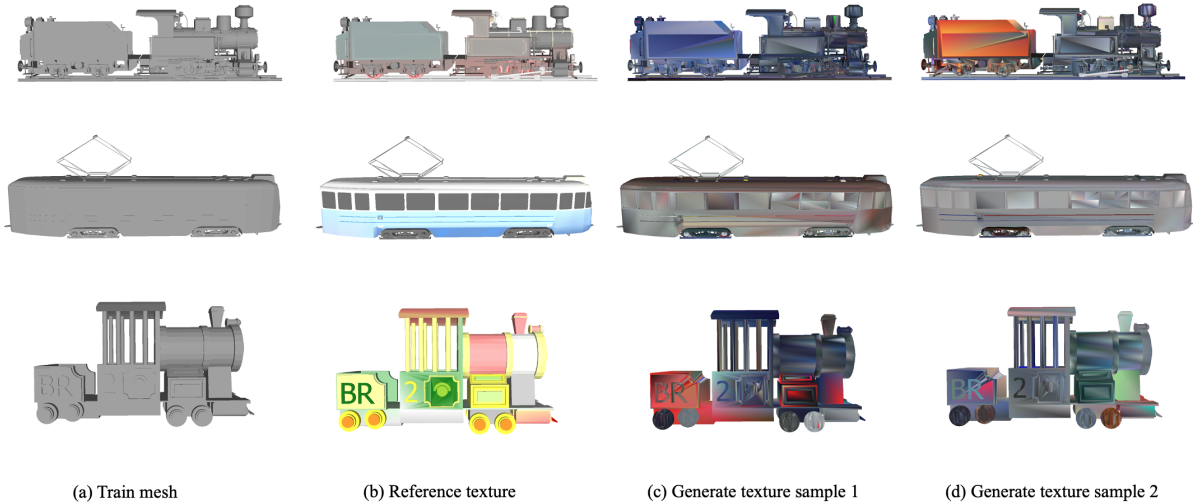


Figure S3. Additional qualitative result on train meshes.



Figure S4. Additional qualitative result on piano meshes.

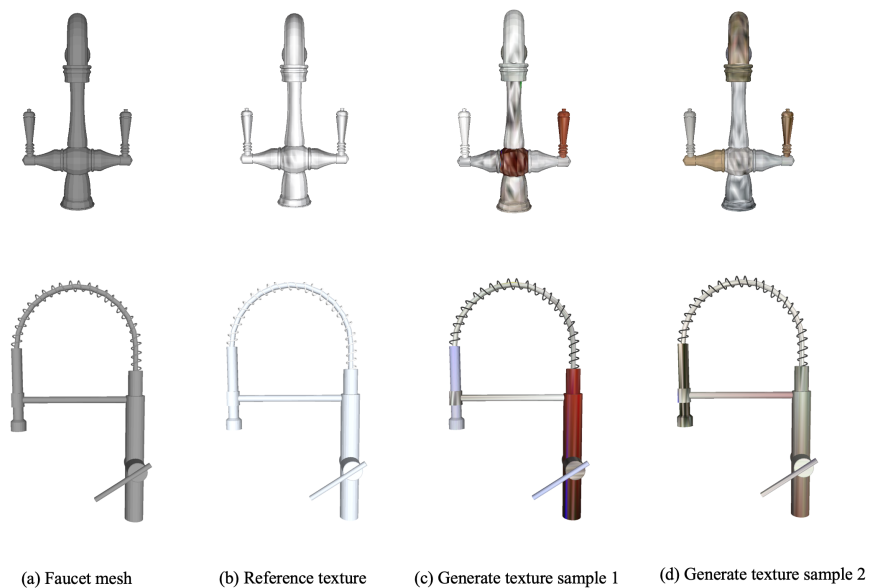


Figure S5. Additional qualitative result on faucet meshes.